

Heavy-Fermion Formation at the Metal-to-Insulator Transition in $\text{Gd}_{1-x}\text{Sr}_x\text{TiO}_3$

M. Heinrich, H.-A. Krug von Nidda, V. Fritsch, and A. Loidl
Institut für Physik, Universität Augsburg, 86135 Augsburg, Germany
(October 28, 2018)

The perovskite-like transition-metal oxide $\text{Gd}_{1-x}\text{Sr}_x\text{TiO}_3$ is investigated by measurements of resistivity, specific-heat, and electron paramagnetic resonance (EPR). Approaching the metal-to-insulator transition from the metallic regime ($x \geq 0.2$), the Sommerfeld coefficient γ of the specific heat becomes strongly enhanced and the resistivity increases quadratically at low temperatures, which both are fingerprints of strong electronic correlations. The temperature dependence of the dynamic susceptibility, as determined from the Gd^{3+} -EPR linewidth, signals the importance of strong spin fluctuations, as observed in heavy-fermion compounds.

PACS: 71.30, 71.27, 76.30

The transition-metal oxides $R\text{TiO}_3$ (where R denotes Y^{3+} , La^{3+} , or some trivalent rare-earth ion) are known as typical Mott-Hubbard insulators with Ti^{3+} in a $3d^1$ electronic configuration [1]. Doping $R_{1-x}A_x\text{TiO}_3$ with divalent alkali-earth ions A like Ca^{2+} or Sr^{2+} partially changes the Ti valence to Ti^{4+} ($3d^0$) and induces metallic behavior at a certain doping concentration x . The metal-to-insulator transition of $\text{La}_{1-x}\text{Sr}_x\text{TiO}_3$ and $\text{Y}_{1-x}\text{Ca}_x\text{TiO}_3$ has been investigated in detail [2, 3]. A critical increase of the Sommerfeld coefficient γ of the specific heat approaching the metal-to-insulator transition has been observed in both compounds with $\gamma \approx 25 \text{ mJ}/(\text{mole K}^2)$ in $\text{Y}_{0.6}\text{Ca}_{0.4}\text{TiO}_3$, indicating an enhancement of the effective electron mass. Heavy-fermion formation has been observed in a number of transition-metal oxides, with $\text{Sr}_{1-x}\text{Ca}_x\text{RuO}_3$ [4] and LiV_2O_4 [5] being the most prominent examples. In the latter two compounds the temperature dependence of the dynamic susceptibility, as probed by the spin-lattice relaxation time in NMR experiments, played a key role in identifying the heavy-fermion behavior. In this letter we investigate the dynamic susceptibility utilizing Gd EPR and provide experimental evidence of heavy-fermion behavior in $\text{Gd}_{1-x}\text{Sr}_x\text{TiO}_3$.

Ceramic samples of $\text{Gd}_{1-x}\text{Sr}_x\text{TiO}_3$ have been calcinated from TiO_2 , SrCO_3 , Gd_2O_3 and Ti_2O_3 powders of high purity (better than 3N) and pressed into pellets. These pellets have been annealed at 1473K under N_2 atmosphere for 15 hours and finally arc-melted under argon atmosphere. For Sr concentrations $x \leq 0.7$ X-ray powder diffraction revealed the proper orthorhombically distorted GdFeO_3 perovskite structure [6]. For $x > 0.7$ the system attains the cubic perovskite structure like pure SrTiO_3 . The volume of the unit cell remains nearly constant at about 235 \AA^3 in the whole concentration range. Susceptibility measurements were performed with a commercial SQUID magnetometer (Quantum Design) in a temperature range $4.2 \leq T \leq 400 \text{ K}$. Pure GdTiO_3 shows a ferrimagnetic susceptibility, which follows a Curie-Weiss law $\chi \propto (T + \Theta)^{-1}$ with $\Theta = 10 \text{ K}$

at high temperatures $T > 100 \text{ K}$, and exhibits an ordering temperature $T_C \approx 28 \text{ K}$. This fits reasonably to the value of 34 K given in literature [7], where the ordered state is reported to show an antiparallel alignment of the ferromagnetically ordered Ti^{3+} spins with respect to the Gd^{3+} spins. With increasing x the Curie-Weiss temperature Θ shows approximately a linear decrease and vanishes for $x \rightarrow 1$, whereas the magnetic order strongly becomes suppressed. Already at $x > 0.1$ no magnetic order was observed for $T \geq 1.7 \text{ K}$ from our EPR measurements reported below. For all samples, the paramagnetic susceptibility is dominated by the contribution of the Gd^{3+} spins ($S_{\text{Gd}} = 7/2$), which is by a factor $S_{\text{Gd}}(S_{\text{Gd}} + 1)/S_{\text{Ti}}(S_{\text{Ti}} + 1) = 21$ times stronger than the contribution of the Ti^{3+} spins ($S_{\text{Ti}} = 1/2$). Comparing the theoretically expected and experimentally observed susceptibility, we obtained that the samples exhibit the correct composition x within an error of $\Delta x \approx 0.02$.

Electrical resistivity, using standard four-probe lock-in technique, and specific heat, using the adiabatic method, were measured in home-built ^4He cryostats in a temperature range $1.5 \leq T \leq 300 \text{ K}$ on bulk samples cut from the arc-melted ingots. Fig. 1 shows the temperature dependence of the resistivity for Sr concentrations $x \leq 0.5$ normalized to the value at $T = 300 \text{ K}$. For pure GdTiO_3 the resistivity strongly increases on decreasing temperature, as it is expected for a Mott insulator. With increasing Sr concentration the resistivity strongly decreases and a metal-to-insulator transition occurs for $x \approx 0.2$. Within the concentration range $0.3 \leq x \leq 0.5$ the resistivity obeys roughly a quadratic temperature dependence, which is demonstrated in the inset of Fig. 1. The observed temperature dependence $\rho - \rho_0 \propto T^2$, instead of the usual phonon contribution $\rho - \rho_0 \propto T^5$, is typical for electron-electron scattering and only observable, if the effective mass of the electrons is strongly enhanced due to electronic correlations like in heavy-fermion systems [8]. At Sr concentrations $x > 0.6$ (not shown in Fig. 1) the system becomes gradually insulating, approaching the band insulator SrTiO_3 [9].

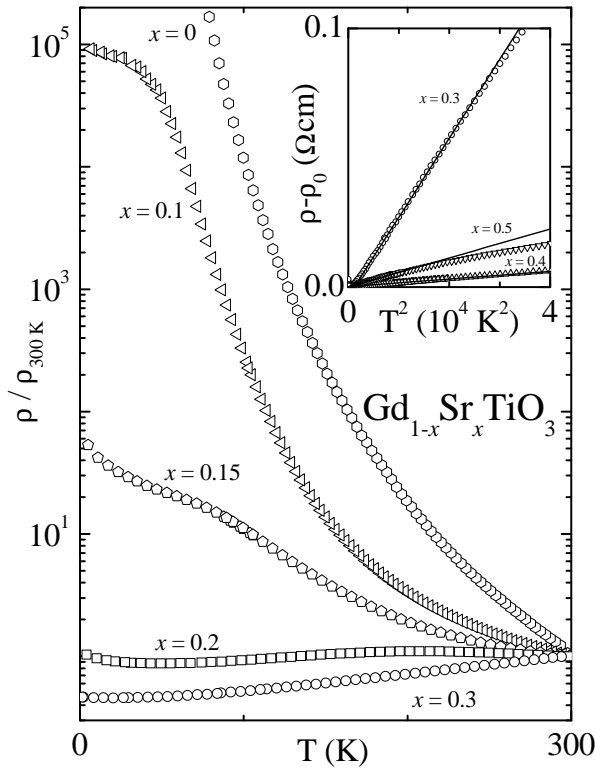


FIG. 1. Temperature dependence of the resistivity $\rho(T)$ for $\text{Gd}_{1-x}\text{Sr}_x\text{TiO}_3$, $0 \leq x \leq 0.3$, normalized to the value at $T = 300$ K. Inset: Resistivity as a function of T^2 for $0.3 \leq x \leq 0.5$ after subtraction of the zero-temperature value ρ_0 . The solid lines indicate a quadratic temperature dependence.

Fig. 2 shows the temperature dependence of the specific heat C for selected samples. Using the representation C/T as a function of T^2 , the linear increase is due to the phonon contribution β , following $C_{\text{ph}} = \beta T^3$, and its extrapolation to $T = 0$ yields the Sommerfeld coefficient γ due to the electronic contribution $C_{\text{el}} = \gamma T$. The increase of the data below 10 K is due to the onset of magnetic order of the Gd spins below 1 K, as we proved for $x = 0.4$ in a $^3\text{He}/^4\text{He}$ -dilution refrigerator. From the extrapolation of the data above 10 K down to $T = 0$ we determined the Sommerfeld coefficient γ for the metallic regime, which is shown in the inset of Fig. 2. Approaching the metal-to-insulator transition from the metallic side, the Sommerfeld coefficient is strongly enhanced up to 50 times with respect to simple metals at $x = 0.2$. This is another hint concerning the enhancement of the effective electronic mass m^* or - in the same sense - of the density of states $N(E_F)$ at the fermi energy, because $\gamma \propto m^* \propto N(E_F)$. Comparing these results to resistivity and specific heat in the well investigated systems $\text{La}_{1-x}\text{Sr}_x\text{TiO}_3$ and $\text{Y}_{1-x}\text{Ca}_x\text{TiO}_3$, we find a quite good agreement. An enhancement of the electronic density of states at low temperatures around the Mott-Hubbard transition is also predicted by theoretical calculations [10]. Hence $\text{Gd}_{1-x}\text{Sr}_x\text{TiO}_3$ is an appropriate system to study the dynamic susceptibility close to a

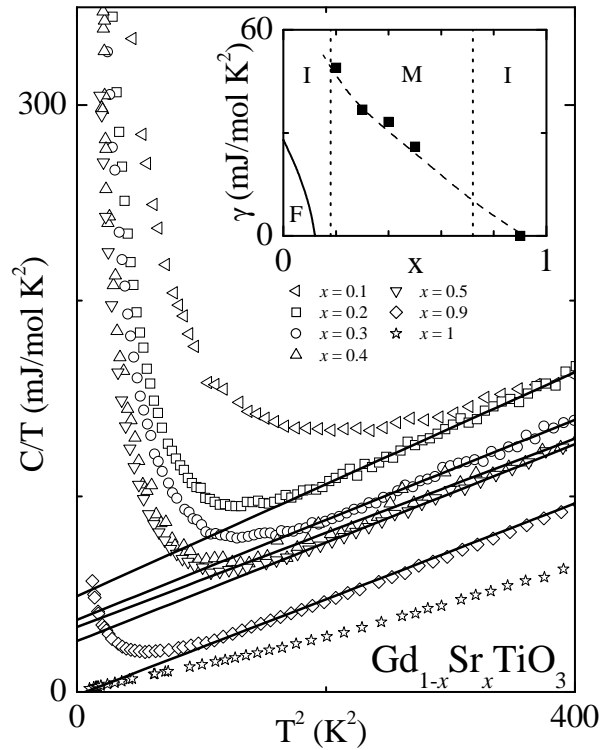


FIG. 2. Temperature dependence of the specific heat $C(T)$ plotted as $C(T)/T$ versus T^2 for $\text{Gd}_{1-x}\text{Sr}_x\text{TiO}_3$. The solid lines indicate a temperature dependence $C(T) = \gamma T + \beta T^3$. The pure compound ($x = 0$) was omitted, as it is dominated by magnetic order in this temperature regime. Inset: Sommerfeld coefficient γ as a function of the Sr concentration x .

Mott-Hubbard transition.

The EPR experiments have been performed at a Bruker ELEXSYS E500-CW spectrometer at X-band frequencies (9.4 GHz) equipped with continuous gas-flow cryostats for He (Oxford Instruments) and N_2 (Bruker) in the temperature range between 4.2 and 680 K. For temperatures down to 1.7 K we used a cold-finger ^4He -bath cryostat. To avoid the influence of the skin effect, which prevents the microwave to enter metallic samples, the arc-melted ingots were powdered, filled in quartz tubes, and embedded in paraffin or NaCl for temperatures below or above room temperature, respectively.

The EPR spectra of all compounds consist of a single exchange-narrowed resonance line of Lorentzian shape with a g value $g \approx 2$. The evaluation of comparable Gd^{3+} spectra has been described in detail in a previous publication [11]. Their intensity follows the Curie-Weiss behavior of the static susceptibility measured with the SQUID magnetometer and comparison with a standard sample showed that it is due to all Gd^{3+} spins. In the Mott-insulating regime $x \leq 0.15$ the resonance linewidth ΔH strongly increases with decreasing temperature below $T < 50$ K, due to the onset of magnetic order. In the minimum near 50 K, it attains a value of about

1 kOe. To higher temperatures $T > 50$ K the linewidth increases with a slightly negative curvature and approximately 2.5 Oe/K. In the metallic regime $0.2 \leq x \leq 0.6$, the linewidth ΔH exhibits a clearly different behavior, which is shown in Fig. 3: Starting at low temperatures the linewidth strongly increases, develops a prominent maximum and decreases again. At temperatures above 150 K the linewidth remains nearly constant ($x \leq 0.4$) or shows a further slight decrease ($x \geq 0.5$). Approaching the metal-to-insulator transition from above ($x \geq 0.2$), the maximum increases and shifts to lower temperatures.

In the following discussion, we confine ourselves to the metallic regime: In metals the transversal spin-relaxation time T_2 equals the longitudinal or spin-lattice relaxation time T_1 . Hence the EPR linewidth $\Delta H \propto 1/T_2$ directly measures the spin-lattice relaxation rate $1/T_1$, which is usually found linear in temperature for simple metals, probing the electronic density of states $N(E_F)$ due to the Korringa law [12]:

$$\Delta H = b \cdot T, \text{ where } b \propto N^2(E_F). \quad (1)$$

However, the temperature evolution of the linewidth observed in $\text{Gd}_{1-x}\text{Sr}_x\text{TiO}_3$ differs completely from the linear Korringa law [12], but it reveals similar features as the Gd ESR [11, 13] and NMR spin-lattice relaxation rate [14] in heavy-fermion compounds. Moreover comparable NMR results have been reported for transition-metal oxides with heavy-fermion formation like LiV_2O_4 [5] and $\text{Ca}_{1-x}\text{Sr}_x\text{RuO}_3$ [4]. In all these systems a second important contribution to the spin-lattice relaxation arises from spin fluctuations of the electronic bath due to the fluctuation-dissipation theorem, which for temperatures large compared to the exciting frequency $k_B T \gg \hbar \omega$ reads

$$\frac{1}{T_1} \propto \frac{T}{\omega} \cdot \text{Im}\chi(\omega, T). \quad (2)$$

Here $\text{Im}\chi(\omega, T)$ denotes the imaginary part of the dynamic susceptibility of the band states represented by the Ti $3d$ electrons in the present case. An appropriate expression for the dynamic susceptibility, which takes the itinerant character of the Ti electrons into account, is given by Ishigaki and Moriya [15, 16], who developed a theoretical description of nuclear magnetic relaxation around the magnetic instabilities in metals. Their results were also used to explain the NMR relaxation rate in $\text{Ca}_{1-x}\text{Sr}_x\text{RuO}_3$ [4]. Ishigaki's simulations of the nuclear spin-lattice relaxation rate $1/T_1$ near a ferromagnetic instability - the Ti spins order ferromagnetically (!) - look quite similar to our linewidth data. Substituting the hyperfine coupling of the nuclear spin with the electronic system by the super-exchange interaction between Gd^{3+} and Ti^{3+} spins, we achieved an analogous expression for the EPR linewidth. Moreover it was necessary, to include the effect of the external magnetic field onto the

magnetic instability [16]. Finally we used the following expression to fit our data:

$$\Delta H = A_{\text{SE}} \cdot \frac{3ty^2}{2(y^3 + h)} + \Delta H_0. \quad (3)$$

The reduced inverse $3d$ susceptibility y is given by an implicit integral equation [15], which has to be iterated numerically. It is characterized by two parameters y_0 and y_1 , respectively: y_0 is proportional to the inverse static susceptibility at zero temperature and therefore vanishes at the magnetic instability. $y_1 \equiv T_0 \cdot y_2$ is proportional to the energy width T_0 ($\sim 0.01 - 0.1$ eV) of the dynamical spin-fluctuation spectrum. Both parameters are normalized to the width T_A (~ 1 eV) of the distribution of the static susceptibility in momentum space. The variable $t = T/T_0$ denotes the reduced temperature. The parameter $h \propto H^2$ describes the influence of the applied magnetic field H . The super-exchange coupling, which is included in the prefactor A_{SE} , is assumed to be temperature independent. The residual linewidth ΔH_0 is due to the contribution of impurities and inhomogeneities in the sample. Hence there are six parameters altogether to describe the temperature dependence of the linewidth.

To obtain a reasonable description of our data, we tried to find a parameter set, where the parameters h - the resonance is found at about $H = 3.4$ kOe for all compounds - and $y_2 \propto (1/T_A)^2$, which is related to the width of the conduction band, attain the same values for all Sr concentrations. The coupling constant A_{SE} and the residual linewidth ΔH_0 were allowed to change slightly. The most important effect was expected to appear in the parameter y_0 , which is directly tuned by the Sr concentration x , and the energy width T_0 of the spin-fluctuation spectrum. The results are drawn as solid lines in Fig. 3 and the respective fit-parameters are listed in Table 1. The fit nicely describes the experimental data at temperatures $T \ll T_0$ and underlines the dominant influence of the $3d$ -spin fluctuations for relaxation near the Mott-Hubbard transition: Indeed the super-exchange coupling and residual linewidth change only slightly within the metallic concentration regime under consideration. Both parameters y_0 and T_0 increase nearly linearly with the Sr concentration x . The critical concentration for the onset of magnetic order ($y_0 = 0$) accompanied by the transition to the Mott insulator is found at $x \lesssim 0.2$ in agreement with the resistivity measurements.

The resonance linewidth at temperatures far below the maximum, which is shown in the upper inset of Fig. 3, exhibits deviations from the linear behavior predicted by the theory. The slope is too small, and for $x \leq 0.4$ one observes even a slight upturn with decreasing temperature instead of the expected linear decrease. These deviations are probably due to the influence of the crystal-electric field or the onset of magnetic order below $T = 1$ K, which both induce a broadening of the resonance line. In the case of a small crystal-electric field the linewidth at low

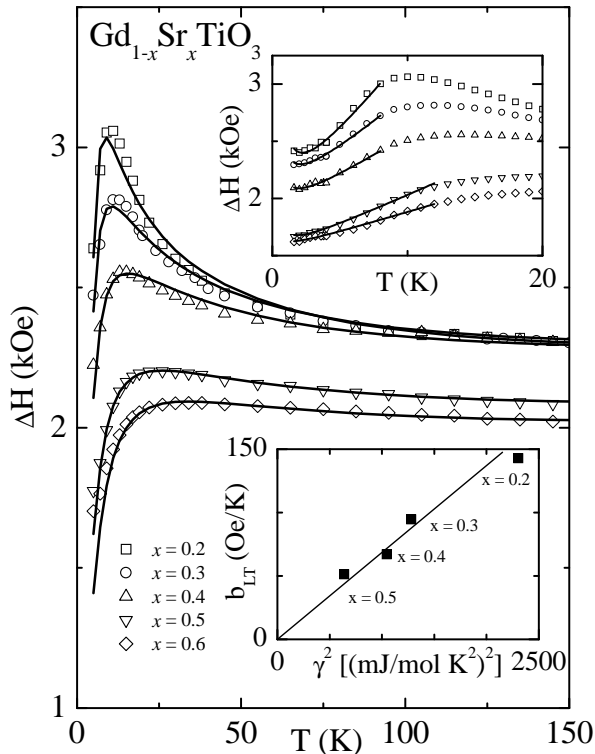


FIG. 3. Temperature dependence of the EPR linewidth $\Delta H(T)$ for $\text{Gd}_{1-x}\text{Sr}_x\text{TiO}_3$ within the metallic regime $0.2 \leq x \leq 0.6$. The solid curves have been calculated from equation (3). The fit parameters are given in table 1. Upper inset: linewidth at low temperatures. The solid lines indicate a temperature dependence following equation (4). Lower inset: Low-temperature Korringa slope b_{LT} as a function of the squared Sommerfeld coefficient γ^2 . The solid line indicates the correlation of b_{LT} and γ^2 .

temperatures follows (solid lines in the upper inset of Fig. 3) [12]

$$\Delta H = b_{\text{LT}} \cdot T + \frac{M_2}{b_{\text{LT}} \cdot T} + \Delta H_0, \quad (4)$$

where M_2 is proportional to the second moment of the crystal-field splitting. It is interesting to compare the low-temperature Korringa slope b_{LT} derived from equation (4) - having in mind the pure Korringa law (1) - with the squared Sommerfeld coefficient γ^2 of the specific heat, as is shown in the lower inset of Fig. 3. The clear correlation of both parameters underlines the enhancement of the electronic density of states $N(E_F)$ at low temperatures in the metallic regime near the Mott-Hubbard transition. It is visible by both macroscopic (γ) and microscopic (b_{LT}) probes.

In conclusion we have shown that the compound $\text{Gd}_{1-x}\text{Sr}_x\text{TiO}_3$ exhibits a metal-to-insulator transition near a Sr concentration $x = 0.2$: Electrical resistivity and specific heat at the transition are in full agreement with the well known systems $\text{La}_{1-x}\text{Sr}_x\text{TiO}_3$ and $\text{Y}_{1-x}\text{Ca}_x\text{TiO}_3$. As Gd^{3+} naturally belongs to the compound, it is well suited for EPR investigations. The

temperature dependence of the Gd^{3+} linewidth in the metallic regime $0.2 \leq x \leq 0.6$ is determined by the Ti^{3+} -spin fluctuations and is well described by the theory of Ishigaki and Moriya for a metal near a ferromagnetic instability. The low-temperature behavior of resistivity, specific heat and ESR linewidth resembles to the properties of heavy-fermion systems, but the enhancement of the effective electronic masses by a factor 50 is weaker than in f-derived heavy fermions, which are dominated by Kondo-compensation effects and where one observes an enhancement factor of 1000.

We are grateful to Dr. E. W. Scheidt, Experimentalphysik III, University of Augsburg, for specific-heat measurements at temperatures below 1 K. This work was supported by the Bundesministerium für Bildung und Forschung (BMBF) under the contract number EKM 13N6917/0 and by the Deutsche Forschungsgemeinschaft within Sonderforschungsbereich 484.

- [1] M. Imada, A. Fujimori, and Y. Tokura, Rev. of Mod. Phys. **70**, 1040, (1998).
- [2] Y. Tokura et al., Phys. Rev. Lett. **70**, 2126 (1993).
- [3] Y. Taguchi et al., Phys. Rev. B **48**, 511 (1993).
- [4] K. Yoshimura et al., Phys. Rev. Lett. **83**, 4397, (1999).
- [5] S. Kondo et al., Phys. Rev. Lett. **78**, 3729 (1996).
- [6] M. Reedyk et al., Phys. Rev. B **55**, 1442 (1997).
- [7] J. E. Greedan, J. Less Common Metals **111**, 335 (1985).
- [8] H. R. Ott: Prog. Low Temp. Phys **11**, 215 (1987).
- [9] M. Cardona, Phys. Rev. **140**, A651 (1965).
- [10] R. Bulla, Phys. Rev. Lett. **83**, 136 (1999).
- [11] H.-A. Krug von Nidda et al., Phys. Rev. B **57**, 14344 (1998).
- [12] S. E. Barnes, Adv. Phys. **30**, 801 (1981).
- [13] B. Elschner and A. Loidl in "Handbook on the Physics and Chemistry of Rare Earth", ed. by K. A. Gschneidner, L. Eyring (Elsevier Science, Amsterdam, 1997) Vol. 24.
- [14] K. Asayama et al., J. Mag. Mag. Mat. **76 & 77**, 449 (1988); N. Büttgen et al., Phys. Rev. B **53**, 5557 (1996).
- [15] A. Ishigaki et al., J. Phys. Soc. Jap. **65**, 3402 (1996).
- [16] T. Moriya, J. Mag. Mag. Mater. **14**, 1 (1979).

| x | $y_0 (\cdot 10^{-4})$ | $T_0 [\text{K}]$ | $A_{\text{SE}} [\text{kOe}]$ | $\Delta H_0 [\text{kOe}]$ |
|-----|-----------------------|------------------|------------------------------|---------------------------|
| 0.2 | 0.1 | 570 | 0.47 | 0.00 |
| 0.3 | 5 | 590 | 0.48 | 0.02 |
| 0.4 | 11 | 610 | 0.46 | 0.15 |
| 0.5 | 19 | 625 | 0.43 | 0.13 |
| 0.6 | 24 | 640 | 0.43 | 0.10 |

TABLE I. Parameters of the fit to the temperature dependence of the EPR linewidth in $\text{Gd}_{1-x}\text{Sr}_x\text{TiO}_3$ following equation (3) with constant values $y_2 = 0.0055 \text{ K}^{-1}$ and $h = 1.9 \cdot 10^{-9}$.